*Acta Cryst.* (1997). D**53**, 765–776

# The Effects of Metal Binding on a Nucleobase: the Experimental Charge Density and Electrostatic Potential in $1H^+$-Adeniniumtrichlorozinc(II) at 123 K and its Relationship to that in Adenine Hydrochloride Hemihydrate

LOUISE M. CUNANE† AND MAX R. TAYLOR*

*Department of Chemistry, The Flinders University of South Australia, GPO Box 2100, Adelaide SA 5001, Australia. E-mail: max.taylor@cc.flinders.edu.au*

(*Received 24 February 1997; accepted 6 June 1997*)

## Abstract

The charge-density distribution in $1H^+$-adeniniumtrichlorozinc(II) has been determined from X-ray diffraction data collected to $\sin\theta/\lambda = 1.32$ Å$^{-1}$ at 123 K. The electrostatic potential, isolated from the crystal lattice, and the deformation density in the nucleobase have been calculated following multipole refinements based on the rigid pseudoatom model of Stewart. These and the molecular dimensions have been compared with results from the charge-density study of adenine hydrochloride hemihydrate by Cunane & Taylor [*Acta Cryst.* (1993). B**49**, 524–530] to determine the effects of metal binding on the nucleobase. The main conclusions are that while the bond lengths and angles in the pyrimidine ring are similar, those in the imidazole ring are significantly perturbed on complexation; lone-pair electron density at N7 is observed in both structures and lies significantly off the plane of the nucleobases; the positive electrostatic potential of the complexed base extends much further from the molecule than in the uncomplexed one and the regions of negative potential at N3 and N7 are depleted in the complexed base. The observed enhancement of positive electrostatic potential in the nucleobase on binding to zinc is presented in support of a model for the mechanism of reversible unwinding of DNA in the presence of zinc ions.

## 1. Introduction

Metal ions are involved in a variety of biological processes and, in particular, participate in several functions of nucleic acid activity. Metal ions can form labile complexes with DNA, binding either to the phosphate groups or the nucleobases, or possibly both, depending on the nature of the metal ion. Coordination of divalent transition metal ions to nucleic acid bases can increase the melting temperature of DNA if the coordination sites are not involved in base-pair hydrogen bonding (Jia & Marzilli, 1991) or can destabilize the double helix at high metal-ion concentration (Duguid, Bloomfield, Benevedes & Thomas, 1993) presumably as a result of competition with hydrogen-bond sites. Zinc ions can bring about the reversible unwinding and rewinding of DNA (Eichhorn & Shin, 1968) and in models proposed for the mechanism of this process (Miller, VanDerveer & Marzilli, 1985; Miller *et al.*, 1986) are believed to bind to the nucleobase *via* N7. Many other examples of metal-to-nucleic acid binding and consequent effects can be found in Sigel & Sigel (1996).

Metal-ion binding to nucleobases is expected to modify the electron distribution in the nucleobase and may lead therefore to changes in hydrogen-bonding capability and electrostatic interactions.

The interactions of some metal ions with purine and pyrimidine bases have been studied using *ab initio* SCF-HF computations with minimal basis sets (Anwander, Probst & Rode, 1987, 1990). The latter paper includes predictions about metal-ion enhancement of hydrogen-bonding potential in base pairs. It is particularly interesting because the results show that some metal ions can be expected to enhance the stability of hydrogen bonding between base pairs and that this increase in stability is related to the distance of the coordination site from the hydrogen bonds. Burda, Šponer & Hobza (1996) have studied the interactions of group Ia, Ib, IIa, and IIb metal ions with adenine and guanine at the HF and second-order MP levels employing all-electron and pseudopotential treatments. Among other things, they have calculated metal—N7 bond lengths. In these *ab initio* calculations the influence of mono-coordinate metal ions was modelled. This is far from the realistic situation *in vivo* where these metal ions would be four-, five- or six-coordinate, and there would, in all likelihood, be interactions between the other coordinated groups and the bases causing the metal ions to be not coplanar with the bases. The values of some of the intramolecular parameters obtained in this way differ significantly from those obtained from crystal structure analyses *e.g.* compare Zn—N7(adenine) of length 1.87 Å (Burda, Šponer & Hobza, 1996) and 1.65 Å (Anwander, Probst & Rode, 1990) with 2.04 (2) Å for the same bond in a 9-methyladenine zinc complex (McCall & Taylor, 1976).

† Present address: Department of Biochemistry and Molecular Biophysics, Washington University School of Medicine, 660 S. Euclid Avenue, Box 8231, St Louis, MO 63110, USA.

Experimental charge-density studies of nucleobases or their derivatives that have been published are: 9-methyladenine at 126 K by Craven & Benci (1981), 1-methyluracil at 123 K by Klooster, Swaminathan, Nanni & Craven (1992), $\beta$-cytidine and cytosine monohydrate (Chen & Craven, 1995) and that of 3′-*O*-acetyl-2′-deoxy-5-methoxymethyluridine at 145 K by Wei, Barton & Robertson (1994).

The X-ray crystal structure of the zinc (II) complex, 1$H^+$-adeniniumtrichlorozinc(II), form (i), was first determined at room temperature by Taylor (1973) from two-circle diffractometer data. The structure was later redetermined from a superior set of four-circle diffractometer data by Taylor, Vilkins & McCall (1989) in order to make a comparison with a room-temperature neutron study (McCall, 1980). The complex exists as discrete adeniniumtrichlorozinc molecules. The adeninium ligand is coordinated to zinc through N7 and is protonated at N1; it is significantly non-planar, being slightly folded along the C4—C5 bond, and the N1—C5 vector. There is a distorted tetrahedral arrangement around zinc, formed by N7 and the three Cl atoms. The Zn—N7 bond makes an angle of 14° with the plane of the imidazole ring. The crystal structure reveals an extensive network of both intramolecular and intermolecular hydrogen bonds. Another crystalline modification of the zinc complex, form (ii), has been reported by Muthiah, Mazumdar & Chaudhuri (1983). The molecule is identical to form (i), within experimental error, except for minor differences in the bonds to the Zn atom.

In this report we present the results of a charge-density study of 1$H^+$-adeniniumtrichlorozinc(II) in which the detailed electron-density distribution, electrostatic potential and accurate molecular geometry of the complex have been determined. These results are compared with those from a similar study of adenine hydrochloride hemihydrate (Cunane & Taylor, 1993) to determine the effects of metal binding on the nucleobase.

## 2. Experimental

Crystals of 1$H^+$-adeniniumtrichlorozinc(II), form (i), $[ZnCl_3(C_5H_6N_5)]$, $M_r$ = 307.9, are monoclinic, space group $P2_1/c$. The unit-cell parameters at room temperature, obtained by Taylor, Vilkins & McCall (1989), were $a$ = 10.844 (4), $b$ = 5.931 (2), $c$ = 15.718 (6) Å, $\beta$ = 90.92 (3)° and $Z$ = 4. Crystals, grown by evaporation of an acidified mixture of zinc chloride solution and adenine in the molar ratio of 16:1, were mounted on 2 mm long glass fibres attached to copper pins. Diffraction data were collected on a CAD-4 diffractometer, with graphite-monochromated Mo $K\alpha$ X-rays ($\lambda$ = 0.71069 Å), from a crystal cooled in a liquid-nitrogen gas stream, held at 123 ± 1 K. Several crystals were screened for quality, and the best specimen, measuring 0.175 × 0.250 × 0.150 mm, mounted on the diffractometer with **b*** tilted at a few degrees from the $\varphi$ axis, was used for data collection. Unit-cell parameters at 123 K obtained from a least-squares fit of 25 reflections, measured at four symmetry-equivalent positions, in the range $18.8 \le \theta \le 34.8°$, were $a$ = 10.857 (1), $b$ = 5.902 (1), $c$ = 15.591 (1) Å and $\beta$ = 90.44 (1)°, $V$ = 999.01 (1) Å$^3$; $D_x$ = 2.047 Mg m$^{-3}$. A total of 17 897 reflections to $\sin\theta/\lambda$ = 1.32 Å$^{-1}$ were measured in the range $-27 \le h \le 27$, $-9 \le k \le 14$, $-38 \le l \le 38$, $\omega/\theta$ scans, variable scan range (1.0 + 0.35 $\tan\theta$)°, aperture size (1.6 + $\tan\theta$) mm. A full sphere of data was collected to $\sin\theta/\lambda$ = 0.77 Å$^{-1}$. This was supplemented by higher order data collected from the $k \ge 0$ hemisphere, selected on the basis of $E$-value calculations from a preliminary refinement and experimental tests, so that $I(hkl)$ was expected to be $\ge 2\sigma(I)$. Three intensity control reflections, (3 2 −4, 2 0 0 and 1 0 −14) monitored every 7200 s of exposure time, showed no long-term trends but there were short-term variations of ±1.5%; data were corrected for this effect. The data were collected in three stages, separated by several weeks, from the same crystal. The final data set, after omitting 892 reflections that had not been remeasured at slow scan speed because they had a negative net peak count after the preliminary fast scan, comprised 16 987 reflections. Absorption corrections were applied, ($\mu$ = 3.286 mm$^{-1}$), Gaussian integration, transmission factors 0.661 (max.) and 0.529 (min.); unique set of 5349 reflections, $R_{int}(F^2)$ = 0.021. The *Xtal* system of crystallographic programs (Hall & Stewart, 1989) was used for all conventional calculations, and the *POP* procedure of Craven, Weber & He (1987), which assumes the rigid pseudoatom model of Stewart (1976), was used for charge-density calculations.

## 3. Refinements

### 3.1. *Conventional refinement*

Starting coordinates for the non-H atoms were taken from the room-temperature study by Taylor, Vilkins & McCall (1989); the H atoms were located in a difference map and were initially assigned isotropic temperature factors 1.5 times that of their parent atoms. Using the full data set, the positional and anisotropic displacement parameters of the non-H atoms and the scale and isotropic extinction factors (Zachariasen, 1967) were refined [final $g = 2.9\ (1) \times 10^3$], and anomalous dispersion corrections applied. The worst affected reflection (2 1 −3) had an extinction correction factor of 0.88. Conventional refinements with program *SFLSX* (Hall, Spadaccini, Olthof-Hazekamp & Dreissig, 1989), using scattering factors for neutral atoms and dispersion corrections from *International Tables for X-ray Crystallography* (1974, Vol. IV), minimizing $\sum w|F_{obs} - F_{calc}|^2_H$ with 128 variables gave $R(F)$ = 0.018, $wR$ = 0.020 and $S$ = 2.237, where $w = 1/\sigma^2(F)$, with $\sigma(F)$ obtained from counting statistics and the usual statistical formulae

associated with the standard deviation of averages. A high-order refinement of a data set of 3047 reflections, with $\sin\theta/\lambda \geq 0.65$ Å$^{-1}$ converged at $R(F) = 0.017$, $wR = 0.015$ and $S = 1.184$.

The title compound has been investigated by neutron diffraction at room temperature by McCall (1980); the bond lengths to H atoms obtained in that study have been used to estimate more accurate H-atom coordinates. The positions of the H atoms were extended along their bond vectors to the neutron bond lengths; the revised H-atom positions were then included in the model but their positional and displacement parameters were held invariant. Further refinement using *CRYLSQ* (Olthof-Hazekamp, 1995), minimizing $\sum w|F^2_{obs} - F^2_{calc}|^2_H$ with 128 variables gave: $R(F) = 0.019$, $wR(F^2) = 0.043$, $S = 2.364$ (full data set, 5349 reflections), and $R = 0.017$, $wR(F^2) = 0.030$ and $S = 1.173$ (high-order data only, 3047 reflections). Difference maps calculated after these refinements gave residual densities of $\Delta\rho_{max} = 0.64$ and $\Delta\rho_{min} = -0.44$ e Å$^{-3}$, and $\Delta\rho_{max} = 0.24$ and $\Delta\rho_{min} = -0.21$ e Å$^{-3}$ for the full and high-order refinements, respectively. Coordinates used to calculate bond lengths and angles came from this last high-order refinement and are presented in Table 1 (Hall, King & Stewart, 1995). These dimensions are consistent with those given in a recent compilation by Parkinson, Vojtechovsky, Clowney, Brünger & Berman (1996). The molecular structure with displacement ellipsoids (those for H derived as above) is shown in Fig. 1.

Table 1. *Non-H-atom coordinates from conventional high-order refinement*

$U_{eq} = (1/3)\Sigma_i\Sigma_j U^{ij} a_i^* a_j^* \mathbf{a}_i.\mathbf{a}_j$.

| | $x$ | $y$ | $z$ | $U_{eq}$ (Å$^2$) |
|---|---|---|---|---|
| C2 | 0.27844 (7) | 0.11798 (13) | 0.37290 (5) | 0.0135 (1) |
| C4 | 0.36845 (5) | 0.25279 (12) | 0.49058 (4) | 0.0104 (1) |
| C5 | 0.28681 (6) | 0.43236 (12) | 0.49847 (4) | 0.0096 (1) |
| C6 | 0.19267 (6) | 0.45616 (12) | 0.43577 (4) | 0.0101 (1) |
| C8 | 0.40705 (6) | 0.43895 (14) | 0.60883 (5) | 0.0130 (1) |
| N1 | 0.19313 (6) | 0.28678 (12) | 0.37572 (4) | 0.0119 (1) |
| N3 | 0.36909 (6) | 0.09337 (12) | 0.42783 (4) | 0.0132 (1) |
| N6 | 0.10979 (6) | 0.61836 (13) | 0.43191 (5) | 0.0145 (1) |
| N7 | 0.31216 (5) | 0.54824 (11) | 0.57401 (4) | 0.0110 (1) |
| N9 | 0.44503 (5) | 0.26141 (12) | 0.56031 (4) | 0.0126 (1) |
| Cl1 | 0.07590 (2) | 0.53685 (3) | 0.71928 (1) | 0.01338 (3) |
| Cl2 | 0.11996 (2) | 1.01888 (3) | 0.57208 (1) | 0.01414 (3) |
| Cl3 | 0.35938 (2) | 0.88164 (4) | 0.74711 (1) | 0.01726 (4) |
| Zn | 0.21410 (1) | 0.76482 (2) | 0.65429 (1) | 0.00942 (2) |

## 3.2. *Multipole refinement*

To determine the charge density in adeniniumtrichlorozinc, least-squares refinements were carried out using the *POP* procedure developed by Craven, Weber & He (1987), which assumes the rigid pseudoatom model of Stewart (1976). All X-ray scattering factors and dispersion corrections were taken from *International Tables for X-ray Crystallography* (1974, Vol. IV).

The refinement strategy was the same as that used in the study of adenine hydrochloride hemihydrate (Cunane & Taylor, 1993) and detailed therein. The invariant cores of the non-H atoms were described by isolated neutral Hartree–Fock scattering curves, except for the Zn and Cl atoms which were assigned the scattering factors for $Zn^{2+}$ and $Cl^-$ and were not refined with multipole parameters. The function minimized was $\sum w|F^2_{obs} - F^2_{calc}|^2_H$. Of the set of eight multipole refinements reported here, the first four were with H atoms found in the difference map and extended to neutron bond lengths; positional parameters and isotropic temperature factors of the H atoms were held invariant. Two weighting schemes were used: scheme 1, with $\sigma$ as for the conventional refinements above; scheme 2, with $\sigma$ modified to $[\sigma^2_{scheme1} + (0.01F^2_{obs})]^{1/2}$. Refinements I (weighting scheme 1) and II (weighting scheme 2) used the complete data set; the scale, type I extinction, and the coordinates, anisotropic harmonic and anharmonic displacement parameters for the non-H atoms were included in the refinement, together with multipole population coefficients to octapole level for non-H and dipole level for H atoms. Refinements III (weighting scheme 1) and IV (weighting scheme 2) used high-order data ($\sin\theta/\lambda \geq 0.65$ Å$^{-1}$) to refine the coordinates and displacement parameters of the non-H atoms, and these were then held fixed, while all the data were used to refine the multipole parameters of all the atoms.

An alternative means of dealing with H atoms when there are no neutron data available at the appropriate temperature is to subject the non-H-atom framework of the molecule to a rigid-body thermal analysis and to subsequently derive effective anisotropic temperature factors for the H atoms. Using the procedure described in Cunane & Taylor (1993), with internal libration axes chosen along the C4—C5, N1—C5, N7—Zn and three

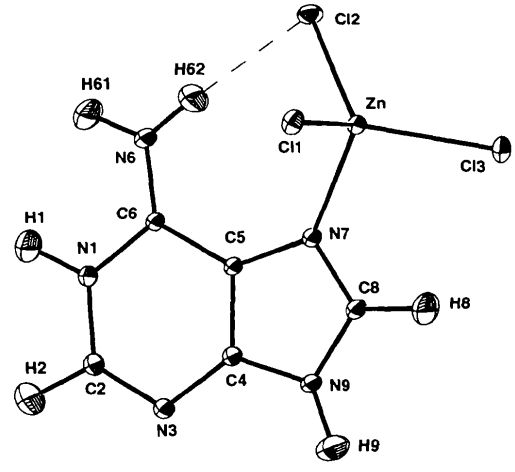


Fig. 1. Atomic labelling in 1*H*-adeniniumtrichlorozinc(II) with displacement ellipsoids at the 50% probability level, at 123 K.

Table 2. *Results of multipole refinements*

| Number | $R(F^2)$ | $wR(F^2)$ | $S(F^2)$ | $R(F)$ |
|---|---|---|---|---|
| I | 0.020 | 0.026 | 1.50 | 0.015 |
| II | 0.020 | 0.030 | 1.29 | 0.015 |
| III | 0.021 | 0.028 | 1.53 | 0.016 |
| IV | 0.021 | 0.031 | 1.32 | 0.016 |
| V | 0.020 | 0.027 | 1.52 | 0.016 |
| VI | 0.020 | 0.030 | 1.30 | 0.015 |
| VII | 0.021 | 0.028 | 1.55 | 0.016 |
| VIII | 0.022 | 0.031 | 1.33 | 0.016 |

Zn—Cl(1,2,3) vectors, giving mean-square librational amplitudes of 7.3 (1.4), 5.8 (8), 2.2 (5), 1.9 (4), 6.4 (5) and 2.0 (5)$^{\circ 2}$, respectively, anisotropic displacement parameters and dipole parameters for H atoms were derived. Refinements V–VIII are analogous to refinements I to IV, but with these anisotropic H-atom parameters and dipole coefficients held at fixed values. In V and VI, the positional parameters and monopoles of H were refined along with the usual parameters on the non-H atoms. In the high-order refinements, VII and VIII, the H-atom coordinates were held at the values obtained in V and VI.

The results of refinements I to VIII are given in Table 2. As with adenine hydrochloride hemihydrate there is very little to choose between these refinements. Coordinates and charge parameters from refinement VIII were used in the charge-density and electrostatic potential calculations which are presented here; refinement VIII was chosen because it was expected that a high-order refinement would result in better deconvolution of thermal parameters from deformation density, and the 'derived' anisotropic H atoms should be the best model available in the absence of neutron diffraction data. Refinement VIII also allows direct comparison with the results presented for adenine hydrochloride hemihydrate. Difference maps, calculated in the least-squares plane through the adenine ring after each of these refinements, showed similar features, the most significant of which is close to the Zn position. Residual densities, $\Delta\rho$, are within the range $-0.29$ and $+0.38$ e Å$^{-3}$.

In all of the above refinements, 'ionic' scattering factors were used for the Zn and Cl atoms. On the face of it, use of $Zn^{2+}$ and $Cl^-$ scattering factors would result in one electron per asymmetric unit not accounted for in the multipole refinement. However, since in the refinement the $ZnCl_3$ fragment has its $\Sigma P_v$ set to zero, it can be expected that the overall sum of the monopole parameters should be approximately zero. For comparison, refinements with neutral scattering factors for Zn and Cl were performed in parallel with refinements I–VIII in order to compare the outcomes. In addition, a refinement parallel to V was run with $Cl^{2/3-}$ and $Zn^{2+}$ scattering factors. In the event, final $R$ values were independent of the scattering factors, as were the values of $S$; the sums of the monopole parameters on the other hand, were affected. For example, from refinement V($Zn^{2+}$ and $Cl^-$), the neutral refinement, and the $Cl^{2/3-}$ scattering-factor refinement, values of $\sum P_v$ were $-0.67$ (29), $-1.02$ (29) and $-1.07$ (29), respectively. It may be that the choice of scattering factor is not crucial, but use of the $Zn^{2+}$ and $Cl^-$ scattering factors was settled upon, after comparison of many refinements showed that the summing of the charge in the asymmetric unit tended more closely to zero with such scattering factors.*

## Results and discussion

### 4.1. *Molecular structure of 1H$^+$-adeniniumtrichlorozinc(II)*

When bond lengths and angles calculated after the conventional high-order refinement (Table 3) and the all-data refinement are compared, it is found that although bond lengths to zinc are all longer as calculated from the high-order refinement, none of these differences are significant. The only difference greater than 3 s.u.'s in the ring bonds is that of N1—C6: 1.370 (1) Å (high-order) and 1.374 (1) Å (all-data). There are no significant differences in bond angles.

Bond lengths and angles were also calculated after multipole refinements.† No significant differences were found when they were compared with those from the conventional refinements. After the treatment of the molecule with rigid-body analysis and the subsequent derivation of anisotropic displacement parameters, and the application of dipole moments to the C—H and N—H bonds, there is quite good agreement between refined H-atom coordinates and those found originally in a difference map and calculated to neutron bond lengths, and left invariant in further refinement. Therefore, it seems that the rigid-body thermal analysis is confirmed as a useful method of describing H atoms in the absence of low-temperature neutron data, and when there are good quality X-ray data available.

Bond lengths to H atoms refined to values not dissimilar from the neutron bond lengths found in the room-temperature neutron study of the zinc complex (McCall, 1980); those obtained in refinement VI are given in Table 4. The C2—H2 and C8—H8 bonds appear a little longer than is reasonable, although they are within three standard deviations of the neutron lengths, while the bonds from nitrogen to hydrogen are in excellent agreement.

* Lists of hydrogen coordinates, displacement parameters and least-squares-planes data, from the conventional high-order refinement, and structure factors from the conventional all-data refinement, have been deposited with the IUCr (Reference: GR0729). Copies may be obtained through The Managing Editor, International Union of Crystallography, 5 Abbey Square, Chester CH1 2HU, England. † From multipole refinements: monopole parameters from refinements I–VIII, multipole population parameters (VIII), refined H-atom coordinates (V and VI), bond lengths to H atoms (VI), final difference map $\Delta\rho = 1/V \sum(F_o - F_{c_{\text{multipole}}} \exp(-2\pi i \mathbf{H}\cdot\mathbf{r})$, where $F_{c_{\text{multipole}}}$ was calculated from a multipole model of the electron density.

Table 3. *Bond lengths (Å) and bond angles (°) in $1H^+$-adeniniumtrichlorozinc(II) from low-temperature high-order conventional refinement (upper) and adenine hydrochloride hemihydrate (lower), the latter from Cunane & Taylor (1993)*

| | | | |
|---|---|---|---|
| Zn—Cl1 | 2.2608 (3) | Zn—Cl2 | 2.2172 (3) |
| Zn—Cl3 | 2.2411 (3) | Zn—N7 | 2.0868 (6) |
| N1—C2 | 1.361 (1) | C5—C6 | 1.416 (1) |
| | 1.371 (1) | | 1.408 (1) |
| N1—C6 | 1.370 (1) | C5—N7 | 1.388 (1) |
| | 1.364 (1) | | 1.380 (1) |
| C2—N3 | 1.308 (1) | C6—N6 | 1.315 (1) |
| | 1.308 (1) | | 1.320 (1) |
| N3—C4 | 1.357 (1) | N7—C8 | 1.328 (1) |
| | 1.353 (1) | | 1.323 (1) |
| C4—C5 | 1.388 (1) | C8—N9 | 1.358 (1) |
| | 1.394 (1) | | 1.365 (1) |
| C4—N9 | 1.365 (1) | | |
| | 1.361 (1) | | |
| Cl1—Zn—Cl2 | 110.92 (1) | Cl2—Zn—Cl3 | 118.96 (1) |
| Cl1—Zn—Cl3 | 111.09 (1) | Cl2—Zn—N7 | 107.61 (2) |
| Cl1—Zn—N7 | 104.34 (2) | Cl3—Zn—N7 | 102.47 (2) |
| Zn—N7—C5 | 135.41 (4) | Zn—N7—C8 | 116.74 (5) |
| C2—N1—C6 | 124.21 (6) | C6—C5—N7 | 132.42 (6) |
| | 123.77 (5) | | 131.61 (5) |
| N1—C2—N3 | 124.69 (7) | N1—C6—C5 | 113.16 (6) |
| | 124.80 (7) | | 113.83 (5) |
| C2—N3—C4 | 112.76 (7) | N1—C6—N6 | 120.41 (6) |
| | 112.42 (5) | | 120.89 (5) |
| N3—C4—C5 | 126.88 (6) | C5—C6—N6 | 126.43 (6) |
| | 127.35 (5) | | 125.28 (6) |
| N3—C4—N9 | 126.41 (7) | C5—N7—C8 | 104.82 (6) |
| | 127.05 (5) | | 103.88 (5) |
| C5—C4—N9 | 106.65 (6) | N7—C8—N9 | 112.63 (6) |
| | 105.59 (6) | | 113.23 (6) |
| C4—C5—C6 | 118.21 (6) | C4—N9—C8 | 106.67 (6) |
| | 117.81 (6) | | 106.72 (5) |
| C4—C5—N7 | 109.21 (5) | | |
| | 110.57 (4) | | |

Table 4. *Bond lengths (Å) to H atoms from multipole refinement VI*

| | | | |
|---|---|---|---|
| N1—H1 | 1.04 (4) | N6—H62 | 0.97 (2) |
| C2—H2 | 1.14 (2) | C8—H8 | 1.13 (2) |
| N6—H61 | 0.98 (2) | N9—H9 | 1.06 (2) |

The adenine part of the zinc complex has been shown previously (Taylor, Vilkins & McCall, 1989) to be significantly non-planar. This has been confirmed at low temperature. Least-squares-planes calculations show that the five atoms which comprise the imidazole ring are coplanar, whereas the pyrimidine ring is puckered. There are folds across N1—C5 and, to a lesser degree, C2—C4. The plane defined by N1—C5—C6 makes an angle of 2.73 (7)° with the plane N1—C2—N3—C4—C5. Similarly the C2—N3—C4 plane is 1.57 (8)° from the plane defined by N1—C2—C4—C5. Between the pyrimidine and imidazole rings, across the C4—C5 bond, there is a fold of 4.80 (3)°. H atoms were excluded from the least-squares-planes calculations.

### 4.2. *Difference density: $X$–$X_{HO}$*

The difference density ($X$–$X_{HO}$), is defined by the expression

$$\Delta\rho = 1/V \sum (F_{obs} - F_{calcHO}) \exp(-2\pi i \mathbf{H}.\mathbf{r}),$$

where $F_{calcHO}$ is the structure factor calculated from a refinement of positional and displacement parameters with high-order data, using a free-atom model. Fig. 2 shows the $X$–$X_{HO}$ difference density obtained from a refinement with data where $\sin\theta/\lambda \geq 0.65$ Å$^{-1}$, plotted in a least-squares plane through the adenine part of the molecule. Bonding density is clearly revealed and lone-pair density at N3 and N7 is visible although not well characterized. Maximum and minimum densities obtained were 0.73 and −0.39 e Å$^{-3}$, respectively.

### 4.3. *Charge density from multipole refinements*

The charge density in adeniniumtrichlorozinc was calculated using electron-population parameters obtained in the multipole refinements. The static deformation density is the difference between the electron density calculated from the pseudoatom (multipole model) and from the spherical Hartree–Fock core for the non-H atoms, and the Stewart, Davidson & Simpson (1965) core for the H atoms. The Slater-type wavefunctions which are used to describe the Hartree–Fock cores were taken from Clementi & Roetti (1974). Fig. 3 shows the deformation density mapped in a least-squares plane through the adenine part of the zinc complex. The maximum bonding electron density is 0.79 e Å$^{-3}$; the maximum s.u. in the charge density is 0.06 e Å$^{-3}$. The degree of ellipticity of

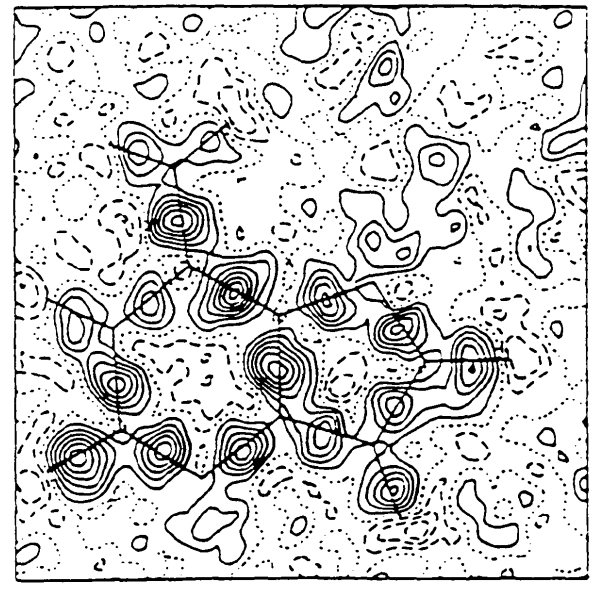

Fig. 2. Difference density, $X$–$X_{HO}$ in the adenine least-squares plane. Contours at 0.1 e Å$^{-3}$

cross sections of deformation density through the midpoints of bonds (Fig. 4*a*) correlates with the bond lengths, the more elliptical cross sections indicating greater $\pi$-character and, therefore, shorter bonds.

Net atomic charges, which are the negatives of the monopole population parameters, are given in Table 5. As expected, the H atoms all carry positive charge; H1 and H9, which are bound to N1 and N9, are more strongly positively charged than the H atoms attached to N6, and to the C atoms. N6 and N7 carry a significant negative charge, while the other N atoms do not. A significant negative charge resides on C8, while the other C atoms are close to neutral.

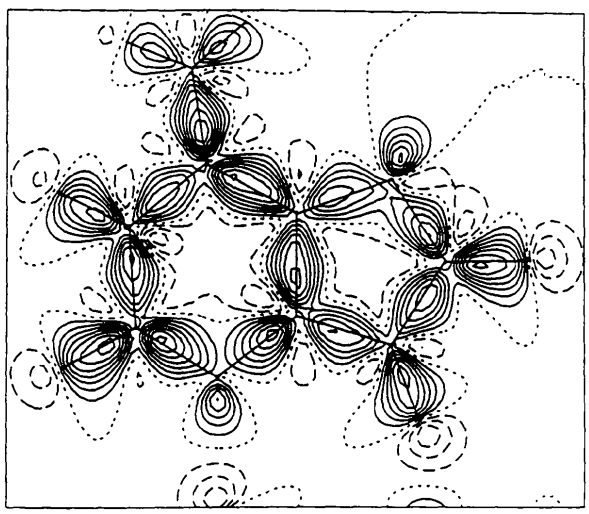

Fig. 3. Deformation density, calculated from a multipole model of the electron density, in the adenine least-squares plane; contour interval 0.1 e Å$^{-3}$

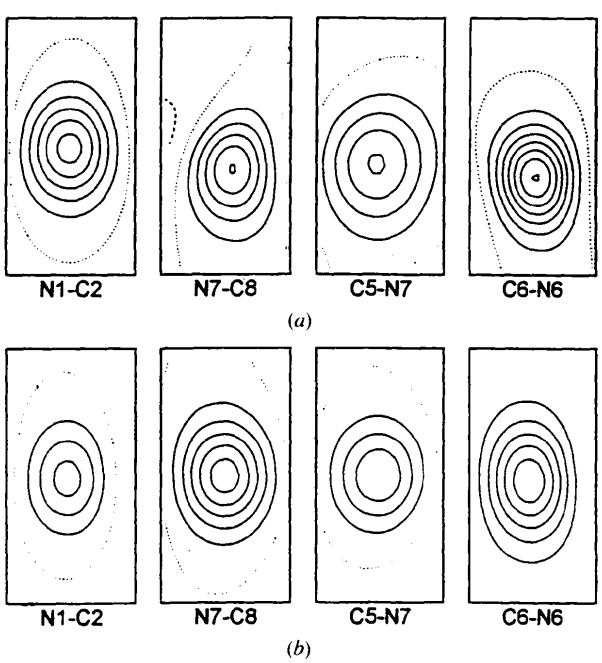


Fig. 4. Cross sections through the deformation density of selected bonds in (*a*) the zinc complex and (*b*) the protonated base, drawn through the mid-points of the interatomic vectors and perpendicular to the plane of the base. Contours at 0.1 e Å$^{-3}$.

Table 5. *Atomic charges ($-P_v \times 10^2$) for those atoms refined with multipolar parameters, averaged over eight multipole refinements*

Values are listed for the protonated adenine moiety of the Zn complex (left) and the hydrochloride (right), the latter being taken from Cunane & Taylor (1993). Standard uncertainties are taken as the maximum of individual contributions, rather than being averaged, as these net charge determinations are all essentially from the same model.

| | | | | | |
|---|---|---|---|---|---|
| N1 | −4 (3) | −14 (2) | C8 | −17 (4) | −14 (2) |
| C2 | −8 (4) | −5 (3) | N9 | −7 (3) | −12 (2) |
| N3 | −3 (3) | −9 (2) | H1 | 27 (2) | 22 (1) |
| C4 | 5 (4) | −14 (2) | H2 | 18 (2) | 14 (2) |
| C5 | −7 (3) | −14 (2) | H8 | 16 (2) | 17 (2) |
| C6 | 10 (3) | −1 (2) | H9 | 26 (2) | 25 (1) |
| N6 | −17 (3) | −18 (2) | H61 | 18 (2) | 16 (2) |
| N7 | −17 (3) | −10 (2) | H62 | 15 (2) | 18 (2) |

### 4.4. *Electrostatic potential*

The charge-density distribution was used to calculate the electrostatic potential in the adenine part of 1$H^+$-adeniniumtrichlorozinc(II). The map of electrostatic potential, calculated in the least-squares plane of the adenine moiety (Fig. 5*a*), reveals regions of negative potential at N3 and N7, and positive potential around the H atoms extending well out into space. The extent of influence of the positive potential is shown in Figs. 5(*b*)–5(*e*), at distances of 1 and 2 Å above and below the adenine plane. The maximum s.u. in electrostatic potential is 0.07 e Å$^{-1}$.

## 5. The effects of metal binding on the nucleobase

In both adenine hydrochloride hemihydrate and 1$H^+$-adeniniumtrichlorozinc(II) the adenine bases are protonated at N1; thus, the principal difference between the two structures, with respect to the bases, is the presence or absence of metal coordination at N7.

### 5.1. *Molecular dimensions*

From a survey of crystallographic studies of metal–nucleobase complexes, Hodgson (1977) concluded that the coordination of a metal ion to a nucleobase does not induce a significant change in the internal ring angle at the site of metal binding. The results of the present study indicate that this is not the case. Moreover, there are other significant differences in bond lengths and other internal angles of the bases when the zinc–adeninium complex and the free protonated base are compared, as Table 3 clearly shows.

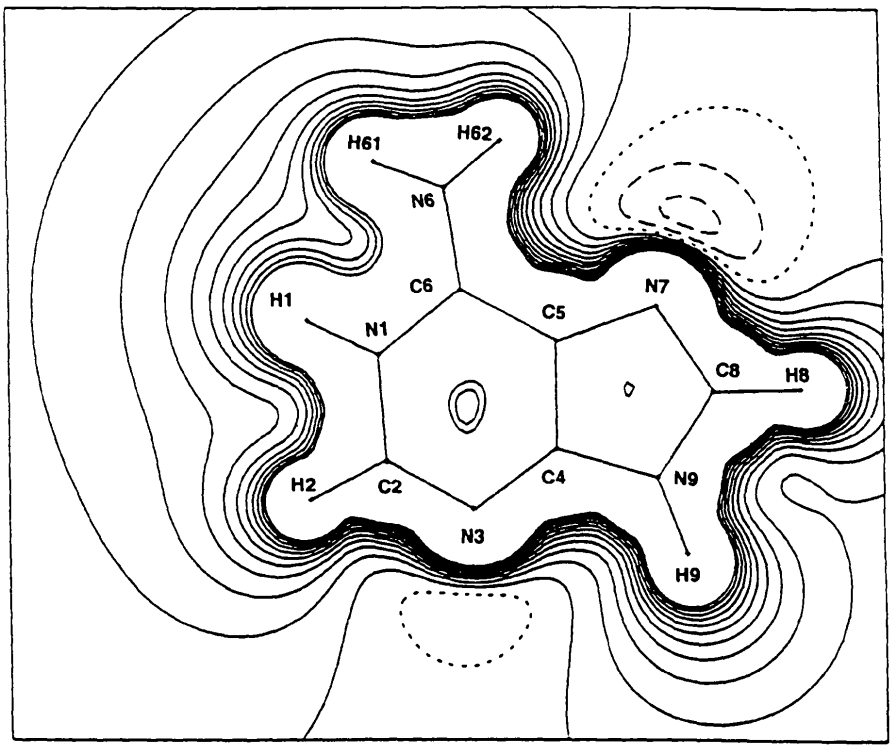


(a)

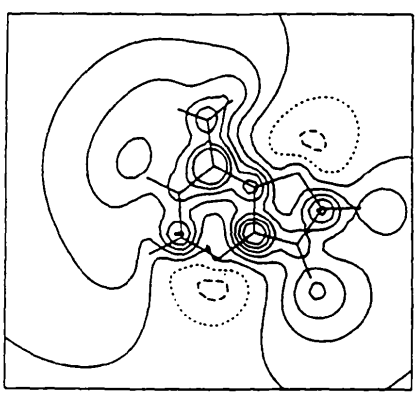

(b)

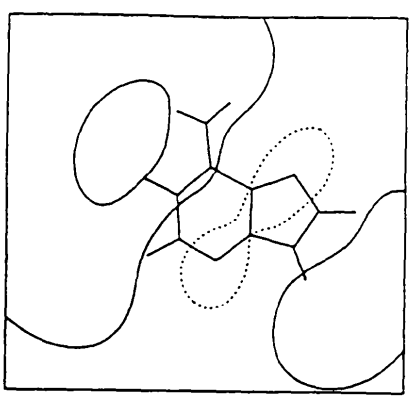

(c)

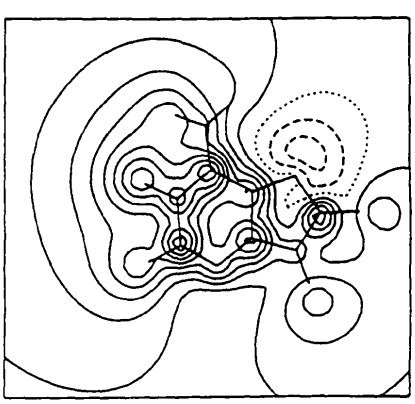

(d)

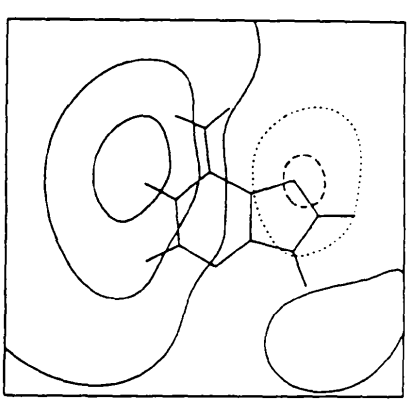

(e)

Fig. 5. Electrostatic potential in $H^+$-adeniniumtrichlorozinc(II), isolated from the crystal lattice, calculated from the multipolar model of the diagram. Contours at 0.1 e Å$^{-3}$. (*a*) $\rho_{def}$ from the multipole model and (*b*) $X$–$X_{HO}$ difference density, for the hydrochloride (left) and the zinc complex (right). The N7—Zn vector is shown, as is the position of H62′.

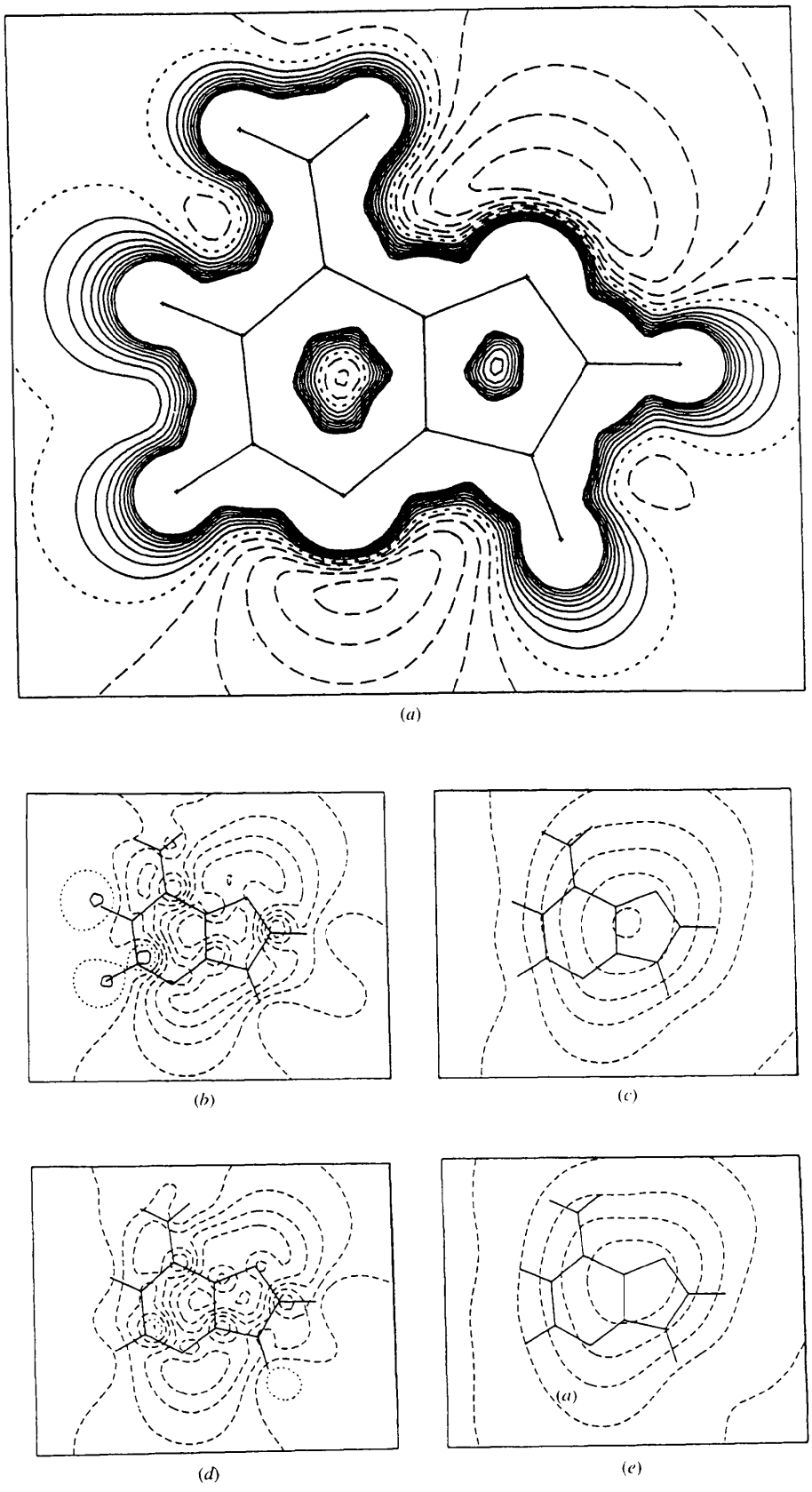


Fig. 6. Electrostatic potential in adenine hydrochloride, isolated from the crystal lattice, calculated from the multipolar model of the charge-density distribution; contours at $0.05\,e\,Å^{-1}$, zero contour is dotted and negative contours dashed. The maximum positive contour drawn is $+0.45\,e\,Å^{-1}$. (*a*) In the adenine plane, (*b*) 1 Å above, (*c*) 2 Å above, (*d*) 1 Å below and (*e*) 2 Å below the adenine plane. [Taken from Cunane & Taylor (1993).]

The internal angles in the imidazole ring at the coordination site N7, and at C5 and C4, differ significantly. The increase at N7 in the Zn complex, of 0.94 (8)°, is reminiscent of the well documented expansion at N upon protonation of these systems. The internal angle at C6 in the pyrimidine ring is significantly reduced, but other internal angles of the pyrimidine ring do not change significantly. The significant increase of 1.15 (9)° at the external angle C5—C6—N6 in the complex is probably due to strain caused by accommodating the intramolecular hydrogen bond N6—H62···Cl2. Other large differences, such as those in external bond angles at N atoms of the purine ring can probably be attributed to the effects of inter- and intramolecular hydrogen bonding in the crystal. There are also differences in the external angles at C2 and C8, where, in both structures, both H2 and H8 are involved in contacts with Cl atoms at distances less than 3 Å. The differences in bond lengths and bond angles are indicative of differences in the extent of double-bond character in the individual bonds, a result of a change in electron distribution within the nucleobase.

The possible resonance forms which contribute to the stability of protonated adenine are depicted in Fig. 7. As noted by Taylor & Kennard (1982) in their survey of the effects of protonation on nucleobases, it can be concluded, from a comparison of bond lengths in neutral and protonated adenine derivatives, that forms II and IV are significant resonance contributors in the protonated base, with smaller contributions from I and III. The shorter C6—N6 and C4—C5 bond lengths and longer N1—C6 and C6—C5 bonds in the complex, when compared with equivalent bonds in the uncomplexed protonated base, suggest that resonance form II may be dominant in the metal complex. It has been shown that N6, C6, N1 and C5 are coplanar, but that this plane deviates from the rest of the pyrimidine ring, which itself is folded with respect to the imidazole ring. Such folding could inhibit electron delocalization over the entire purine ring.

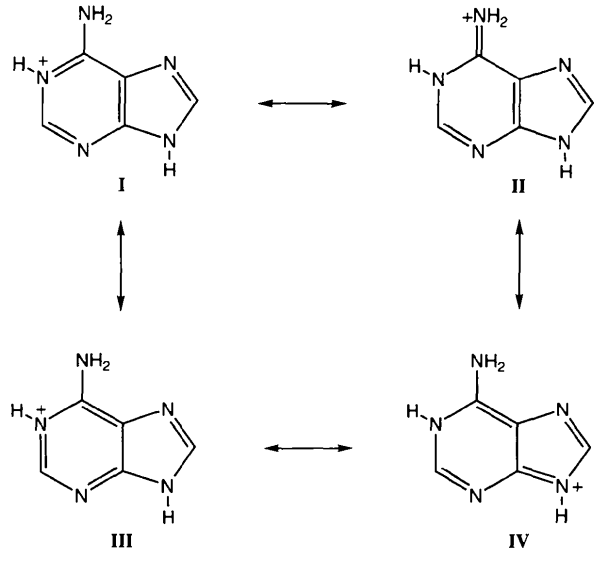


Fig. 7. Possible resonance contributors to N1-protonated adenine.

### 5.2. *Deformation and difference maps*

The deformation-density maps plotted in the least-squares plane of the nucleobase in both the zinc complex (Fig. 3) and the uncomplexed base [see Fig. 4 of Cunane & Taylor (1993)] are rather similar in overall appearance. In the latter, however, the N1—C2 bond seems lacking in electron density compared with the complex; this is the bond which has the largest difference in bond length between the two structures.

In the hydrochloride, the appearance of the amino group in the deformation density and $X$–$X_{HO}$ difference density maps is similar with considerably higher density in the N6—H61 bond than in N6—H62 (Cunane & Taylor, 1993). In the zinc complex there is a more even distribution of density in the two bonds (Figs. 2 and 3), and the deformation density, but not the difference density, is higher in N6—H62 than in N6—H61. It may be that the depletion in overall density in the amino group of the zinc complex is due to the formation of the N6—H62···Cl2 intramolecular hydrogen bond. We have no explanation to offer for the higher deformation density in N6—H62 compared with N6—H61 in the zinc complex other than to note that the deformation density is more model dependent than the difference density and is perhaps, therefore, not so reliable.

In Fig. 4, cross sections of $\rho_{def}$ for selected bonds in the two compounds are depicted. Small differences between the uncomplexed base and the metal-complexed one, such as those seen in N1—C2 and N3—C4, lend further support to the conclusion that there has been a redistribution of electron density in the nucleobase upon metal coordination. They also support the earlier statements (§5.1) about resonance contributors. For example, the C6—N6 bond shows marked ellipticity, confirming that canonical form (II) (Fig. 7) is a major contributor to the structure. On the other hand, the C5—N7 bond is more circular in cross section, and in all four resonance contributors is a single bond.

In Fig. 8, sections have been plotted perpendicular to the plane of the base at N7 to show the lone-pair deformation density and the $X$–$X_{HO}$ difference density at the metal coordination site; included for comparison, are similar sections for the hydrochloride. In the complexed base, the maxima of both the lone-pair deformation density and the difference density are not coplanar with the base and the difference density lies further from a coplanar disposition than does the N7—Zn vector. In the hydrochloride, the maximum in the lone-pair difference density is similarly situated with respect to the vector

N7—H62′. The atom H62′ in the hydrochloride is involved in a hydrogen bond to N7 with H···N distance of 1.945 (2) Å; its position is shown in Fig. 8 and it lies 0.3 Å above the plane of the page. The difference density is not as model dependent as the deformation density, and may be a better indicator of the spatial distribution of the lone-pair density than the latter. The fact that the lone-pair difference density is not in the plane of the base in both complexed and uncomplexed forms suggests that this is a real effect. Of course, it must be kept in mind that this is a situation which will be influenced to some extent by the crystalline environment – the arrangement of electron density is a result of energy minimization in the crystal. The similarity of the difference density at N7 in the complex and the uncomplexed base leads one to speculate that the coordination of zinc to the base is essentially an 'ionic' type of bonding interaction. (This supports the use of the $Zn^{2+}$ scattering factor in the multipole refinements.) It is difficult to rationalize the increase in the internal angle at N7 on binding to zinc, other than to conclude that it is brought about as part of the overall redistribution of electron density in the base. The lone-pair density at N3 in the complex is not defined clearly enough to enable conclusions to be drawn about any possible effect of metal complexation on its position. It is possible that this lone-pair density is delocalized into the ring, resulting in poorly characterized extra-ring density.

Table 5 shows the net atomic charges for the complexed and the uncomplexed bases, averaged over the eight multipole refinements. One notable feature in both structures is the polarity of the C8—H8 bond, an observation that is consistent with the well known acidity of H8 in purines. Ring atoms N1, C4, C5 and C6 are more positive in the zinc complex and N7 more negative, while the charges on the other atoms are approximately the same, within experimental error, for both the base and the complex. These differences may be the result of an electron-withdrawing effect caused by the coordination of the electrophile zinc(II) at N7.

### 5.3. *Electrostatic potential*

The electrostatic potential of the nucleobase isolated from the crystal structure, calculated from the experimental charge distribution, is remarkably different in the two compounds (Figs. 5 and 6). The regions of negative potential at N3 and N7 are depleted in the zinc complex compared with the uncomplexed base. The lines of positive equipotential are much more compact in the uncomplexed nucleobase compared with its zinc complex, where the positive potential extends well out from the molecule. In the regions above and below the planes of the base, negative potential is still visible at 2 Å from the uncomplexed base, but it is mostly positive potential present at this distance from the base coordinated to zinc. The nucleobase is expected to be both a $\sigma$-electron donor and a $\pi$-electron acceptor at N7. The increase in positive electrostatic potential in the complexed base indicates that the $\sigma$-donor property outweighs the $\pi$-acceptor property and that the $ZnCl_3^-$ moiety is acting as a net electron acceptor. This causes the protons to become more acidic and electropositive, *via* an electron-withdrawing effect. This conclusion is supported by the

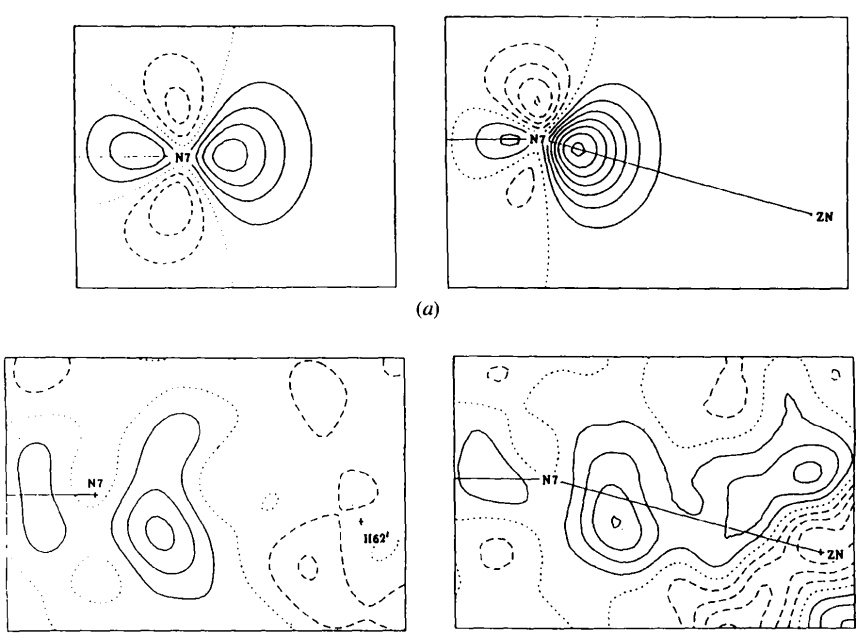


Fig. 8. Sections normal to the plane of the base and containing the C5—N7—C8 bisector; the base plane is drawn at left in each diagram. Contours at 0.1 e Å$^{-3}$. (*a*) $\rho_{def}$ from the multipole model and (*b*) $X$-$X_{HO}$ difference density, for the hydrochloride (left) and the zinc complex (right). The N7—Zn vector is shown, as is the position of H62′.

effects on the atomic charges in the nucleobase. Thus, coordination to the metal ion, with its associated chloro ligands in this case, appears to deactivate the nucleobase to further electrophilic attack.

### 5.4. *Comparison with ab initio studies*

The *ab initio* studies of Anwander, Probst & Rode (1987, 1990) and Burda, Šponer & Hobza (1996), in which the effect of metal-ion binding to nucleobases has been examined, all, quite reasonably, deal with neutral ligands. Unfortunately, this makes detailed comparisons between their results and those presented here, where the adenine ligand is protonated, unrewarding. It is worth noting that the increase in positive electrostatic potential observed in this study parallels the findings of Anwander, Probst & Rode and lends support to the conclusions from their study. Nevertheless it should be emphasized that these *ab initio* studies in general appear to give rise to molecular geometries that appear to be far from those expected for coordination compounds in their minimum-energy configurations.

## 6. Comments on a possible mechanism for the reversible unwinding of DNA by zinc ions

Eichhorn & Shin (1968) proposed that the phenomenon of reversible unwinding of DNA in the presence of zinc ions occurs *via* a metal-ion crosslink between the strands of the double helix. Crystallographic studies of bivalent metal complexes of nucleic acid components have confirmed the affinity of the metal ions for various sites on the nucleobases, and the results have been used in an attempt to support Eichhorn & Shin's proposal. In the majority of studies, N7 was found to be the favoured site for zinc coordination to N9-substituted adenine and guanine derivatives, and it was therefore inferred that this atom might be involved in the binding of zinc by nucleic acids. Interesting exceptions to this observation were found in structures determined by McCall & Taylor (1975, 1976), where zinc was found to bind to the N1 atom in one 9-methyladenine derivative, and to N1 and N7 of adjacent bases, in another. Since N1 is directly involved in the A·T base-pair hydrogen bond, it was suggested that metal binding between N1 and N7 of adenine in an interstrand crosslink might be a means of zinc binding to DNA during the denaturation process, thus supporting Eichhorn & Shin's proposal.

An alternative model for the reversible unwinding of DNA by zinc has been proposed by Miller, VanDerveer & Marzilli (1985). They suggested an *intra*strand crosslink of two adjacent guanine bases, zinc binding through N7. This model would not require the disruption of base-pair hydrogen bonds as in the *inter*strand crosslink. They also highlight another problem with the interstrand crosslink mechanism – labile metal species, such as zinc, show no particular preference for the binding of adenine with thymine, or guanine with cytosine, when both ligands are present; it could, therefore, be assumed that some slippage of the strands might occur when they are linked by a labile species, possibly bringing about base mismatches on rewinding.

Can the effects of the coordination of zinc to protonated adenine, which were observed in this experimental charge-density study, be related to the interaction of zinc ions with nucleic acids? One must first assume that zinc bound to the N7 position of adenine in DNA would induce similar effects to those seen in this model crystallographic study. It is difficult to make any inference from the differences in molecular dimensions and deformation density, beyond the conclusion that there has been a redistribution of bonding electron density in the nucleobase on binding to zinc. The electrostatic potential maps, however, are a qualitative, clear visual indicator of the considerable effect that such electronic changes might have on the hydrogen-bonding capability of the base. Hydrogen bonding is essentially electrostatic in character and any changes in the electrostatic properties of the species involved are likely to affect this interaction in some way.

The observed increase in electropositivity of the base on binding to zinc will, therefore, enhance the hydrogen-bonding interactions between bases across the DNA strands. At the points where zinc is coordinated there may be locally strengthened base-pairing, which may remain in place during denaturation when DNA is heated; this would help to maintain the base pairs in register, so that when cooled, the unwound coils may rewind with the correct base-pairing, resulting in complete renaturation. This proposition lends strong support to the model of Miller *et al.* (1986) who predicted that an intrastrand crosslink between two adjacent guanine bases would in fact produce such an effect. While the subject of this study is adenine, it is probable that guanine would be affected in an analogous manner on binding to zinc. The strong affinity of zinc for the N7 site in guanine and adenine, and purine–purine base-stacking being the most favourable base-stacking interaction (Saenger, 1984), also supports the model of zinc binding through N7 on adjacent purine bases, although some local conformational changes in the helical twist would be necessary to bring this about (Miller *et al.*, 1986).

The authors wish to thank Professor B. M. Craven of the University of Pittsburgh for his invaluable advice and suggestions and for making it possible for one of us (LMC) to work for a short time in his laboratory. This research was supported by a grant from the Australian Research Council.

### References

Anwander, E. H. S., Probst, M. M. & Rode, B. M. (1987). *Inorg. Chim. Acta*, **137**, 203–208.

Anwander, E. H. S., Probst, M. M. & Rode, B. M. (1990). *Biopolymers*, **29**, 757–769.

Burda, J. V., Šponer, J. & Hobza, P. (1996). *J. Phys. Chem.* **100**, 7250–7255.

Chen, L. & Craven, B. M. (1995). *Acta Cryst.* **B51**, 1081–1097.

Clementi, E. & Roetti, C. (1974). *At. Data Nucl. Data Tables*, **14**, 177–478.

Craven, B. M. & Benci, P. (1981). *Acta Cryst.* **B37**, 1584–1591.

Craven, B. M., Weber, H.-P. & He, X. (1987). *The POP Procedure: Computer Programs to Derive Electrostatic Properties from Bragg Reflections.* Technical Report TR-87–2. Department of Crystallography, University of Pittsburgh, USA.

Cunane, L. M. & Taylor, M. R. (1993) *Acta Cryst.* **B49**, 524–530.

Duguid, J., Bloomfield, V. A., Benevides, J. & Thomas, G. J. Jr (1993). *Biophys. J.* **65**, 1916–1928.

Eichhorn, G. L. & Shin, Y. A. (1968). *J. Am. Chem. Soc.* **90**, 7323–7328.

Hall, S. R., King, G. S. D. & Stewart, J. M. (1995). Editors. *XTAL3.4 User's Manual.* Perth: Lamb.

Hall, S. R., Spadaccini, N., Olthof-Hazekamp, R. & Dreissig, W. (1989). *SFLSX XTAL2.6 User's Manual*, edited by S. R. Hall & J. M. Stewart. Universities of Western Australia, Australia, and Maryland, USA.

Hall, S. R. & Stewart, J. M. (1989). Editors. *XTAL2.6 User's Manual.* Universities of Western Australia, Australia, and Maryland, USA.

Hodgson, D. (1977). *Prog. Inorg. Chem.* **23**, 211–254.

*International Tables for X-ray Crystallography* (1974). Vol. IV. Birmingham: Kynoch Press.

Jia, X. & Marzilli, L. G. (1991). *Biopolymers*, **31**, 23–44.

Klooster, W. T., Swaminathan, S., Nanni, R. & Craven, B. M. (1992). *Acta Cryst.* B**48**, 217–227.

McCall, M. J. (1980). PhD thesis, The Flinders University of South Australia, Australia, pp. 126–160.

McCall, M. J. & Taylor, M. R. (1975). *Biochim. Biophys. Acta*, **390**, 137–139.

McCall, M. J. & Taylor, M. R. (1976). *Acta Cryst.* B**32**, 1687–1691.

Miller, S. K., Marzilli, L. G., Dörre, S., Kollat, P., Stigler, R.-D. & Stezowski, J. J. (1986). *Inorg. Chem.* **25**, 4272–4277.

Miller, S. K., VanDerveer, D. G. & Marzilli, L.G. (1985). *J. Am. Chem. Soc.* **107**, 1048–1055.

Muthiah, P. T., Mazumdar, S. K. & Chaudhuri, S. (1983). *J. Inorg. Biochem.* **19**, 237–246.

Olthof-Hazekamp, R. (1995). *CRYLSQ. XTAL3.4 User's Manual*, edited by S. R. Hall, G. S. D. King & J. M. Stewart. Perth: Lamb.

Parkinson, G., Vojtechovsky, J., Clowney, L., Brünger, A. T. & Berman, H. M. (1996). *Acta Cryst.* D**52**, 57–64.

Saenger, W. (1984). *Principles of Nucleic Acid Structure*. New York: Springer-Verlag.

Sigel, A. & Sigel, H. (1996). Editors. *Metal Ions in Biological Systems*, Vol. 32, *Interactions of Metal Ions with Nucleotides, Nucleic Acids and Their Constituents*. New York: Dekker.

Stewart, R. F. (1976). *Acta Cryst.* A**32**, 565–574.

Stewart, R. F., Davidson, E. R. & Simpson, W. T. (1965). *J. Chem. Phys.* **42**, 3175–3187.

Taylor, M. R. (1973). *Acta Cryst.* B**29**, 884–890.

Taylor, M. R., Vilkins, L. M. & McCall, M. J. (1989). *Acta Cryst.* C**45**, 1625–1626.

Taylor, R. & Kennard, O. (1982). *J. Mol. Struct.* **78**, 1–28.

Wei, Y., Barton, R. & Robertson B. (1994). *Acta Cryst.* B**50**, 161–174.

Zachariasen, W. H. (1967). *Acta Cryst.* **23**, 558–564.